ACS OMEGA

Open Access

http://pubs.acs.org/journal/acsodf

Article

Cobalt Oxide Nanoparticle Synthesis by Cell-Surface-Engineered Recombinant *Escherichia coli* and Potential Application for Anticancer Treatment

Ashokkumar Kumaravel, Turbasu Sengupta, Padmanaban Sathiyamoorthy, Jaehoon Jeong, Sung Gu Kang, and Soon Ho Hong*

Cite This: *ACS Omega* 2024, 9, 31373−31383

Read Online

ACCESS | Metrics & More | Article Recommendations | Supporting Information

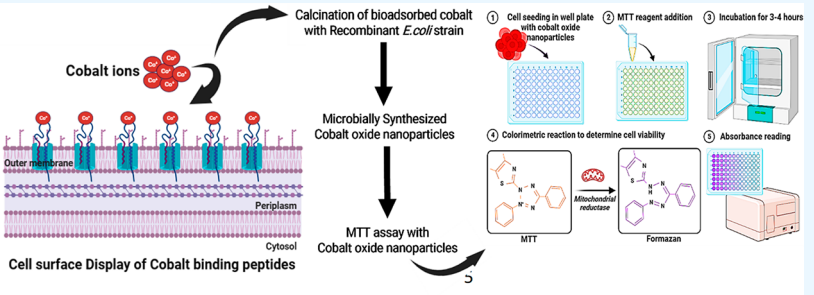

ABSTRACT: Cell surface display engineering facilitated the development of a cobalt-binding hybrid *Escherichia coli*. OmpC served as the molecular anchor for showcasing the cobalt-binding peptides (CBPs), creating the structural model of the hybrid OmpC−CBPs (OmpC−CP, OmpC−CF). Subsequently, the recombinant peptide's cobalt adsorption and retrieval effectiveness were evaluated at various concentrations. When subjected to a pH of 7 and a concentration of 2 mM, OmpC−CF exhibited a significantly higher cobalt recovery rate (2183.87 mol/g DCW) than OmpC−CP. The strain with bioadsorbed cobalt underwent thermal treatment at varying temperatures (400 °C, 500 °C, 600 °C, and 700 °C) and morphological characterization of the thermally decomposed cobalt nanoparticle oxides using diverse spectroscopy techniques. The analysis showed that nanoparticles confined themselves to metal ions, and EDS mapping detected the presence of cobalt on the cell surface. Finally, the nanoparticles' anticancer potential was assessed by subjecting them to heating at 500 °C in a furnace; they demonstrated noteworthy cytotoxicity, as evidenced by IC_{50} values of 59 μg/mL. These findings suggest that these nanoparticles hold promise as potential anticancer agents. Overall, this study successfully engineered a recombinant *E. coli* capable of efficiently binding to cobalt, producing nanoparticles with anticancer properties. The results of this investigation could have significant implications for advancing novel cancer therapies.

1. INTRODUCTION

Cobalt, a versatile d-block transition metal, is pivotal in various industrial sectors, mainly the acrylic and ceramic industries.[1] Additionally, it has applications as an electrocatalyst in hydroformylation, gasification, and thermal decomposition reactions. Moreover, cobalt is indispensable in metallurgy, paints, batteries, electroplating, and electronics. The global battery industry's escalating demand led to a surge in cobalt mining activities, with annual production steadily increasing from 700 to 1200 tons per year between 1995 and 2005 and subsequent continuous growth.

During this growing demand for and application of cobalt, nanoscience emerged as a dynamic interdisciplinary domain with immense promise.[2] The synthesis of cobalt nanoparticles encompasses four distinct methods: physical, chemical, physiochemical, and biological. Each presents unique challenges and requires innovative solutions. Among these, the microemulsion technique stands out for its capacity to fine-tune crucial nanoparticle properties, including size, shape, distribution, and composition. Notably, microemulsion technologies offer extensive parameter adjustment capabilities. Researchers have successfully produced cobalt nanoparticles, approximately 80 nm in size, with a face-centered cubic crystal structure, using plant extracts and red-green algae extracts.[3] Microbiological processes have also proven effective in producing stable nanoparticles, expanding the scope to copper, titanium, zinc, alginate, gold, magnesium, and silver.[4,5] The enduring importance of cobalt oxide (Co_3O_4) remains evident

Received: December 21, 2023
Revised: June 19, 2024
Accepted: June 26, 2024
Published: July 9, 2024

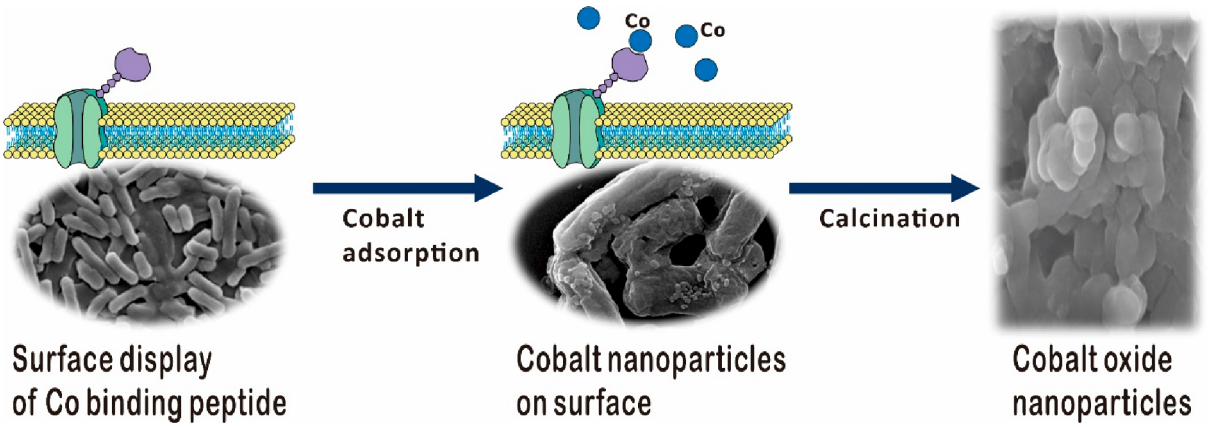

Figure 1. Schematic illustration of the microbial synthesis of cobalt oxide nanoparticles by cell surface display.

in applications like lithium-ion batteries, gas sensors, magnetic storage, and supercapacitors.[3]

Cobalt nanoparticles hold immense potential across diverse applications, including fuel cells, catalysis, medicine, microelectronics, targeted therapies, and drug delivery.[6−9] The magnetic properties of cobalt nanostructures are of particular significance and are paving the way for innovative approaches to utilizing nanoparticles in targeted drug delivery systems.[10,11] Furthermore, due to their unique physicochemical characteristics, cobalt nanoparticles are promising candidates for sensing various chemicals.[12] However, previous research has focused on cobalt resistance.[13−18] Studies on the microbial production of cobalt oxide nanoparticles remain limited. This study aimed to pioneer the production of cobalt oxide nanoparticles using genetically modified strains.

Recent research endeavors have concentrated on leveraging cell surface display as a novel method for anchoring heavy metal-binding proteins or peptides to bacterial surfaces.[19] This approach involves expressing heterologous peptides as fusion proteins with various anchoring motifs on microbial cell surfaces, typically consisting of cell surface proteins or their fragments. Depending on the properties of the passenger and carrier proteins, researchers can utilize C-terminal fusion, N-terminal fusion, or a sandwich fusion method.[19] Microbial cell surface display applications span from developing live vaccines and peptide library screening to bioconversion using whole-cell biocatalysts and bioadsorption. For example, activating the CusSR two-component synthetic genetic circuit on the cell surface has been employed to sense metal and remove copper by regulating the histidine kinase domain and OmpR response in periplasmic metal-sensing receptors upon Cu^{2+} recognition.[20] Another instance involved enhancing mercury (Hg) uptake in *Escherichia coli* cells by displaying the mercury-binding protein MerR on the cell surface.[21] Synthetic phytochelatins applied to the surface of modified *Moraxella* sp.[22] resulted in a more than 10-fold increase in mercury adsorption.

In this study, we introduce a novel cobalt adsorption system formed by affixing cobalt-binding peptides to the C-terminus of shortened OmpC, enabling the synthesis of cobalt nanoparticles, as illustrated in Figure 1. Various characterization techniques, including X-ray diffraction (XRD), field emission scanning electron microscopy (FE-SEM), energy dispersive spectrometry (EDS), Fourier transform infrared (FT-IR), and Raman spectroscopy, were employed to analyze the cobalt nanoparticles synthesized on the surface of engineered *E. coli*. Subsequently, cobalt oxide nanoparticles were synthesized through calcination and analyzed for their anticancer activity using a 3-(4,5-dimethylthiazol-2-yl)-2,5-diphenyl-2H-tetrazolium bromide (MTT) assay.

2. MATERIALS AND METHODS

2.1. Bacterial Strains and Media. The genetic engineering and cobalt adsorption processes utilized *E. coli* DH5α (Enzynomics) as the host organism. These strains were cultivated at 37 °C with agitation at 250 rpm in Luria−Bertani (LB) medium (comprising 10 g/L bacto-tryptone, 5 g/L bacto-yeast extracts, and 10 g/L NaCl), supplemented with 100 mg/L of ampicillin as an antibiotic. Table 1 provides a comprehensive list of the bacterial strains and plasmids employed in this study.

Table 1. List of Bacterial Strains and Plasmids Used in This Study

Strain/ Plasmid	Relevant genotype/property	source
	E. coli strains	
DH5α	MSDS_CP010_DH5α Chemically Competent *E. coli*	Enzynomics
	Plasmids	
pBAD30	Amp^R	NEB[a]
pBADCP	pBAD30 containing OmpC−CP	This work
pBADCF	pBAD30 containing OmpC−CF	This work

[a]New England Biolabs, Beverly, MA, USA.

2.2. Construction of the Cobalt-Binding Peptide Cell Surface Display System. The OmpC−CP and OmpC−CF genes were cloned into the pBAD30 plasmid using SacI and XbaI restriction enzymes. This process led to the construction of pBADCP and pBADCF. The peptides were fused to the truncated OmpC at the C-terminus, specifically at the eighth loop (993rd bp). An extra linker (AEAAAKA) enhanced cell surface display stability between the OmpC and CBPs. To attach the cobalt-binding peptides, CP (18 amino acids long: GMVPSGASTGEHEAVELR) and CF (a 7-amino acid fragment of CP: TGEHEAV), Polymerase chain reaction with the T100TM thermal cycler from Bio-Rad Laboratories (Hercules, CA, USA) and N-Taq polymerase from Enzynomics was employed. Table 2 lists the primers utilized in this study. Subsequently, the recombinant plasmids were transformed into *E. coli* DH5 cells were cultivated in an LB medium.

https://doi.org/10.1021/acsomega.3c10246
ACS Omega 2024, 9, 31373−31383

Table 2. Primers Used in This Work

Name	Sequence (5′ to 3′)
CF-F	GAATTTATGAAAGTGAAAGTGCTGAGCCTGCTG
CP-R	TTAGCGCAGTTCCACCGCTTCATGTTCGCCGGTGCTCGCGCCGCTCGGCACCATGCCCGCTTTCGCCGCCGCTTCCGCCATGTTTTTTGTTGAAGTAGTAGGTAGCACC
CF-R	TTACACCGCTTCATGTTCGCCGGTCGCTTTCGCCGCCGCTTCCGCCATGTTTTTTGTTGAAGTAGTAGGTAGCACC

Arabinose was used to stimulate the expression of the recombinant protein OmpC−CBPs. The ara promoter regulates the induction (Figure 2A).

2.3. SDS-PAGE Expression Evaluation. The recombinant strain was cultured in an LB medium overnight. Afterward, each LB medium underwent a 100-fold dilution for the subsequent subculture. When the subculture achieved an OD600 of 0.5, diverse concentrations of arabinose ranging from 0 to 1% were introduced into the culture medium. The cells were allowed to grow for 6 h. Afterward, the recombinant strains were collected via centrifugation at 13,000 rpm for 10 min. They were then agitated in B-7 M urea buffer at room temperature for 30 min. The supernatant was cleared of cell debris through centrifugation at 8000 rpm. The outer membrane fractions were separated from the cell pellet by adding 10 mM Tris-HCl (pH 7.5) and letting the suspended cells sit at 4 °C overnight. Finally, the lifted membrane fractions were examined using 12% (w/v) sodium dodecyl-sulfate polyacrylamide gel electrophoresis (SDS-PAGE) and stained with Coomassie brilliant blue R-250 (Bio-Rad Laboratories, Hercules, CA, USA).

2.4. Computational Modeling of the Cobalt-Binding Domain. The 3D generation engine of the pepfold (PEPFOLD3) peptide prediction server[23−25] is employed to predict the lowest energy structures of peptides. This prediction tool utilizes a rapid Markov model suboptimal conformation sampling method to determine a peptide's structure from its amino acid sequence. The tool assumes a neutral pH during structure prediction. The best model for each peptide is selected from a list of predicted structures and further analyzed using *ab initio* computational modeling. To identify the optimal binding sites for the Co^{2+} ion within the peptide, we utilized the LEGO module of the ABCluster (version 1.5.1) package[26−28] combined with Gaussian 16 software.[29] ABCluster is reliable software that uses the artificial bee colony (ABC) algorithm to predict the global minima structure. The global minimum search was performed on a 3 × 3 × 3 three-dimensional lattice with a neighboring distance of 2.5 Å. Given the sizes of the peptides and the multitude of potential conformations, we conducted global minima searches at the semiempirical PM6 level.[30]

Furthermore, the fixed positions of hydrogen atoms throughout the simulation were maintained for each peptide. Multiple runs of the ABCluster code were conducted to ensure reliability, generating approximately 1000 isomers for each peptide until all the individual simulations pointed to the same global minima. To accurately predict the binding energy and related thermodynamic parameters, the global minima structures of the peptide-Co^{2+} complex and the peptide predicted by PEPFOLD3 were optimized using the B3LYP functional,[29] all without constraints. The optimization process employed the 6-31G basis set for C, H, N, O, and S atoms and the LANL2DZ-ECP basis set for the Co^{2+} ion,[29] while the SMD solvation model[31] was applied in an aqueous medium. Furthermore, adjustments were made manually to the number of hydrogen atoms within the peptide structures in both the primary and acidic regions of the leading and side chains of the amino acids of the peptide, ensuring an accurate representation of the structure at a neutral pH. The binding energies of the Co^{2+} ion with the peptide in this study were calculated using the following equation, considering a temperature of 298.15 K and a pressure of 1 atm:

https://doi.org/10.1021/acsomega.3c10246
ACS Omega 2024, 9, 31373−31383

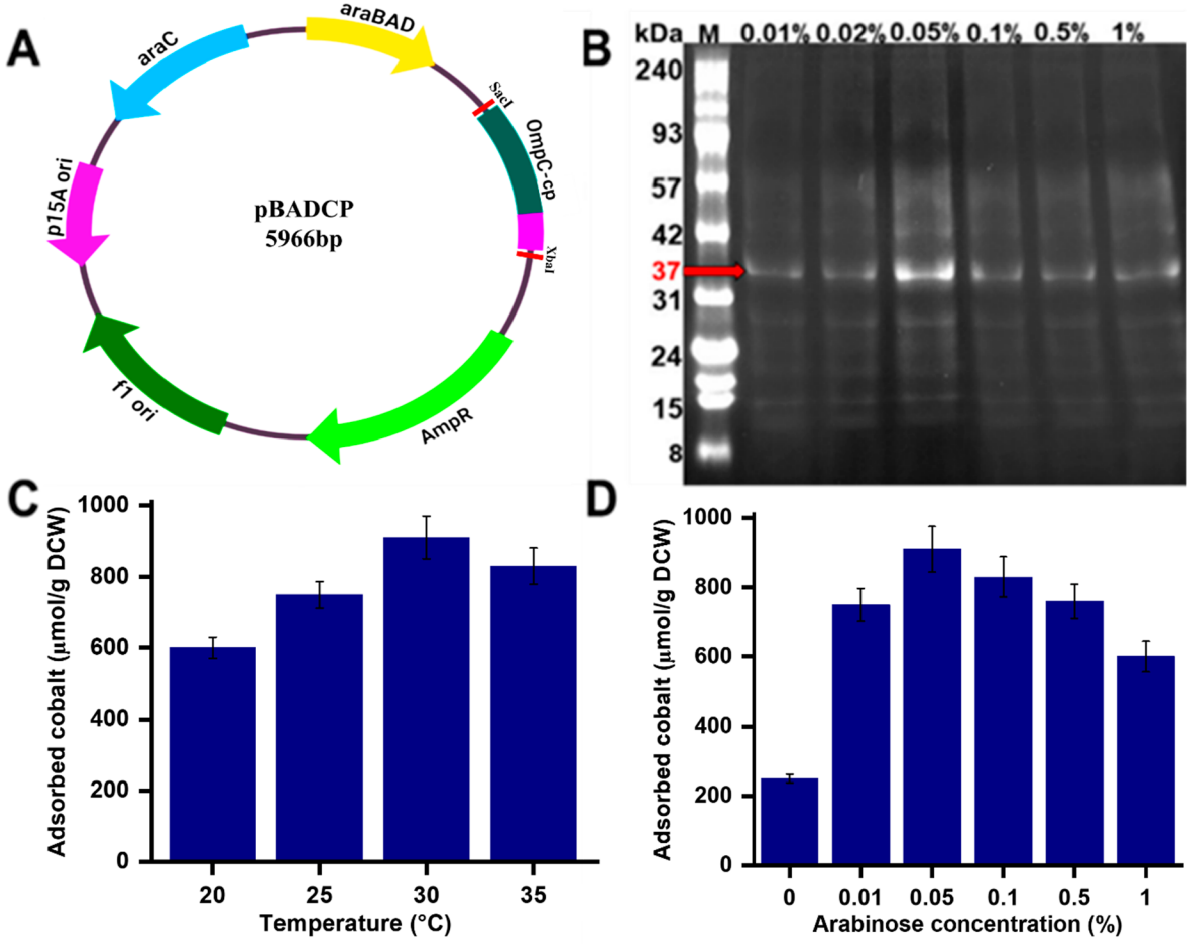

Figure 2. Construction of cobalt binding peptide fused with OmpC at pBAD30 and optimization of its expression conditions. (A) Plasmid construction of cobalt binding peptide (pBADCP) fused with OmpC at pBAD30. (B) SDS-PAGE analysis of recombinant protein *E. coli* (pBADCP) (37 kDa). (C) The effect of temperature toward cobalt adsorption on *E. coli* (pBADCP) with 1 mM $CoCl_2$. (D) The impact of arabinose concentration toward cobalt recovery on *E. coli* (pBADCP) with 1 mM $CoCl_2$.

$$E_{pep} + E_{Co^{2+}} - E_{pep-Co^{2+}\ complex}$$

A higher (more positive) value of the Co^{2+} ion's binding energy with the peptide, represented by the E values for the energies of the peptide fragments, the Co^{2+} ion, and the peptide-Co^{2+} complex, indicates a more vital interaction between the cobalt ion and the peptide. Additionally, we thoroughly examined the normal vibration modes for all optimized structures to confirm their reality and the absence of imaginary modes, thereby validating that the optimized systems corresponded to true energy minima rather than saddle points.

2.5. Cobalt Bioadsorption and analysis. At 37 °C, the recombinant strains containing pBAD30CP and pBAD30CF grew overnight in LB medium supplemented with 100 mg/L of ampicillin. The cultures from the preceding night underwent a 100-fold dilution in fresh LB medium and continued to grow until the optical density, denoted as OD600, reached 0.5. The 0.05% arabinose was introduced to cell cultures, and the strains were maintained at 30 °C for 6 h. The strains underwent centrifugation and exposure to cobalt metal chloride concentrations ranging from 0.25 mM to 5 mM for 2 h at 30 °C while agitating at 250 rpm. The isolates received two consecutive rinses with a 0.85% (w/v) saline solution before being subjected to treatment with 0.1 M HCl for 30 min in a shaker operating at 30 °C and 250 rpm to elute the cobalt ions bound to the cell surfaces. The adsorption of the finest recombinant strain, with *E. coli* DH5α serving as a control, was assessed using an ICP-OES instrument (Agilent Technologies).

2.6. Assessment of the Characteristics of Cobalt Nanoparticles. This process involved collecting cobalt through bioadsorption via calcination at various temperatures (400 °C, 500 °C, 600 °C, and 700 °C). The calcination procedure commenced following a 12 h incubation of arabinose-induced cells in a metal chloride solution. Subsequently, the cells underwent a 24 h water bath at 80 °C, facilitating cobalt binding to the cells. Afterward, a centrifuge collected the metal-bound cell pellets. These pellets underwent calcination at different temperatures in a furnace, following a freeze-drying step at −80 °C. The calcinated oxide samples from the muffle furnace were subjected to various characterization methods, including XRD, FE-SEM, EDS, FT-IR, and Raman spectroscopy analysis.

3. RESULTS AND DISCUSSION

3.1. Construction of the Cobalt-Binding Peptide Display System. The cell membrane exterior exhibited the

https://doi.org/10.1021/acsomega.3c10246
ACS Omega 2024, 9, 31373−31383

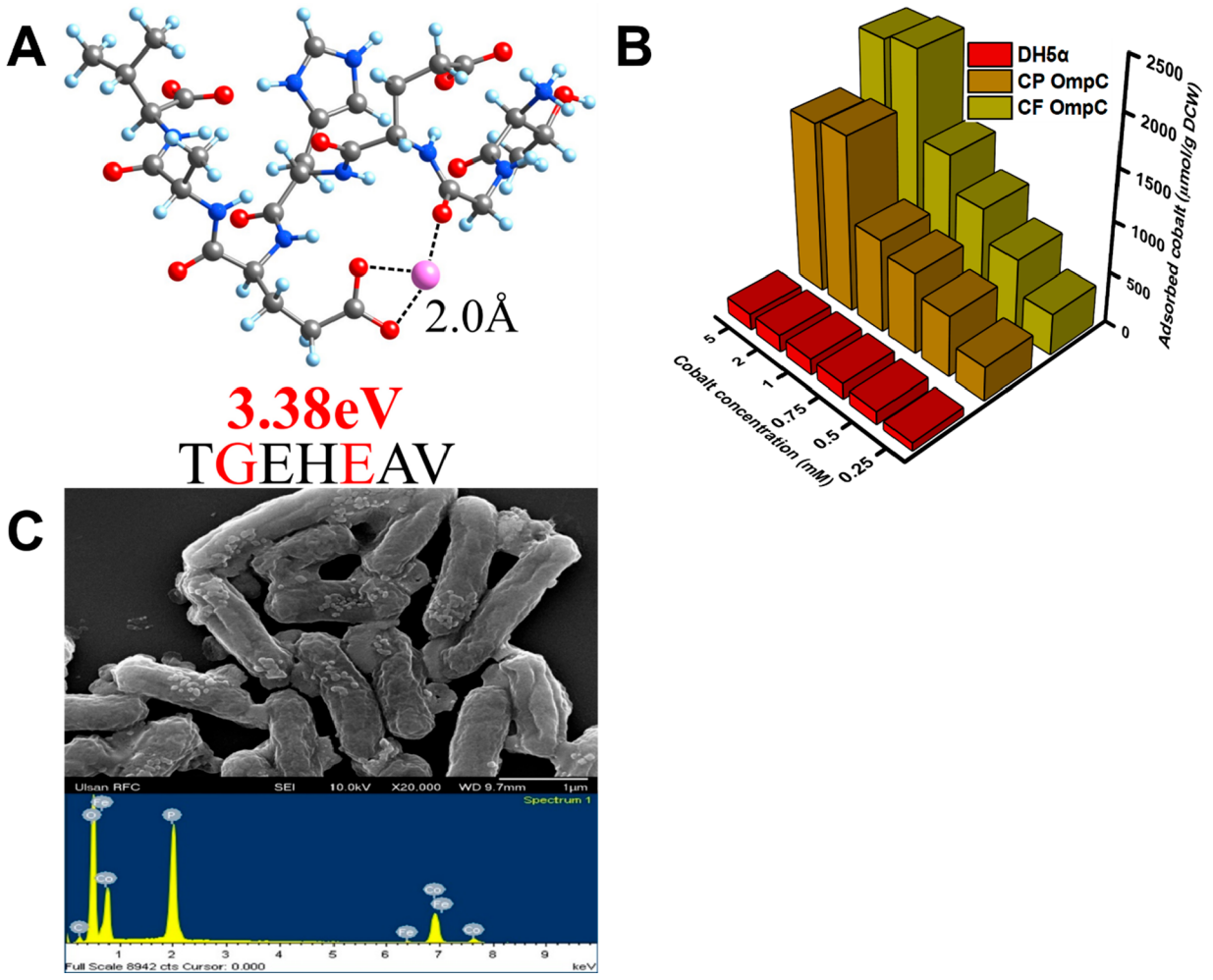

Figure 3. (A) The DFT optimized structure of Co^{2+} with peptide fragment TGEHEAV. The best binding sites and binding energy (eV) are shown in red. The average binding distances (Å) of cobalt atoms with nearby binding sites are shown in black. (B) The adsorption of cobalt by the *E. coli* (pBADCP and pBADCF) with different concentrations of cobalt ranges from 0.25 mM to 5 mM. (C) FE-SEM and EDS analysis for *E. coli* (pBADCF) after adsorption.

cobalt-binding peptide while employing OmpC as an anchoring motif, allowing recombinant *E. coli* to recover cobalt from the environment. The cobalt-binding peptide was attached to the truncated OmpC's C-terminus at the 993rd base pair. The pBADCBPs plasmids, controlled by the arabinose promoter, were constructed for this purpose. Expressing a heterologous protein in *E. coli* typically induces metabolic instability, resulting in decreased protein expression, cell growth, and stability of the recombinant plasmid. Consequently, identifying optimal growth and expression conditions is crucial. The effects of arabinose concentration and culture temperature on the expression of the OmpC−CP peptide were investigated. Arabinose concentration varied from 0.0% to 1.0%, and the temperature was adjusted between 20 and 35 °C to optimize the expression of the OmpC−CP peptide. Subsequently, the recombinant peptide expression levels for OmpC−CP were analyzed using SDS-PAGE (Figure 2B). The optimal expression occurred at an arabinose concentration of 0.05%. Expression levels declined with increasing arabinose concentrations. In cobalt adsorption experiments conducted at different temperatures, increased cobalt adsorption was observed as the temperature rose to 30 °C, which decreased with further temperature increases. The highest cobalt adsorption, 910 μmol/g DCW, was achieved at 30 °C (Figure 2C). The effect of different arabinose concentrations on cobalt adsorption was also investigated. The maximum cobalt adsorption of 1150 μmol/g DCW was observed at 0.05% of arabinose concentration (Figure 2D) with a 1 mM cobalt chloride concentration.

3.2. Computational Modeling of the Cobalt-Binding Domain. Utilizing the selected small-size peptide fragment TGEHEAV, the optimal binding sites for Co^{2+} ions through the utilization of ABCluster in conjunction with density functional theory (DFT) calculations were predicted. This peptide fragment was selected based on studies documenting significant cobalt-binding peptide motifs as M(X)9H.[32] The Co^{2+} ion exhibited a crucial coordination pattern: it coordinated with three oxygen atoms from two neighboring amino acids within the TGEHEAV peptide fragment. The most robust binding energy observed was 3.38 eV, which occurred with the oxygen atoms of glycine and glutamic acid. The Co^{2+} ion bound to these oxygen atoms in a near-tetrahedral coordination fashion, and the average Co−O distance was approximately 2.0 Å, as depicted in Figure 3A. In the case of the TGEHEAV peptide complexes, the average binding energy of Co^{2+} with oxygen atoms ranged from 1.04 to 1.13 eV. These findings indicate that the TGEHEAV peptide

https://doi.org/10.1021/acsomega.3c10246
ACS Omega 2024, 9, 31373−31383

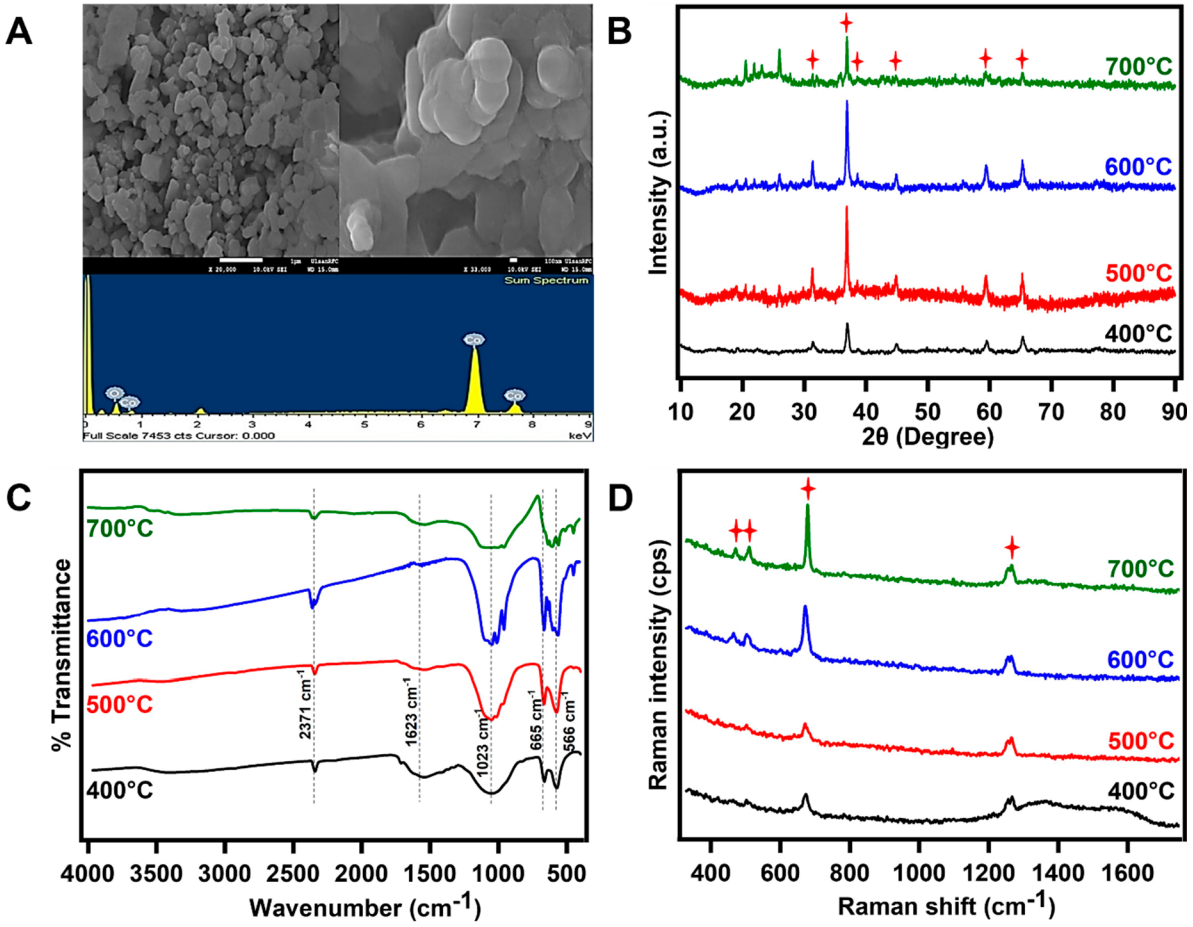

Figure 4. *E. coli* (pBADCF) recovered cobalt's calcinated samples at different temperatures (400 °C, 500 °C, 600 °C, and 700 °C). (A) FE-SEM and EDS for *E. coli* (pBADCF) recovered cobalt oxide nanoparticles, calcinated at 500 °C. (B) X-ray diffraction. (C) FT-IR spectrum. (D) Raman spectrum.

fragment is a promising candidate for future studies exploring cobalt ion binding.

3.3. Evaluation of *E. coli* (pBADCF) cobalt adsorption. The adsorption ability of the newly found cobalt-binding peptide CF and the original cobalt-binding peptide CP was tested. *E. coli* DH5α, *E. coli* (pBADCP), and *E. coli* (pBADCF) were cultured with varying concentrations of $CoCl_2$ (ranging from 0.25 mM to 5 mM) at pH 7. When these strains incubated in a 2 mM cobalt solution, *E. coli* (pBADCF) adsorbed 2183 ± 200 μmol/g DCW of cobalt, whereas *E. coli* (pBADCP) adsorbed 1700 ± 170 μmol/g DCW (as shown in Figure 3B). As the cobalt concentration in the medium increased from 0.25 mM to 2 mM, cobalt adsorption increased and reached saturation, with further increases in cobalt adsorption up to 5 mM. These findings indicate that *E. coli* (pBADCF) exhibited approximately 28% higher cobalt adsorption capacity than *E. coli* (pBADCP). Furthermore, it is observed about 23% higher adsorption compared to recombinant cells of *Acidithiobacillus ferrooxidans* rusticyanin and approximately 60% higher adsorption compared to *A. ferrooxidans* licanantase under a 1 mM induced cobalt concentration.[33] In contrast, when compared to both of our cobalt peptides at a 0.25 mM induced cobalt concentration, *Candida guilliermondii* bioadsorption capacity is six times lower (14.73 μg/g DCW), and *Rhodotorula calyptogenae* adsorption is eight times lower.[34] It is important to note that the wild-type *E. coli* DH5α showed negligible cobalt adsorption.

After the recombinant strain *E. coli* (pBADCF) adsorbed cobalt, we examined it using FE-SEM and EDS to determine the adsorbed metal and elucidate its structure. Following adsorption, we rinsed and lyophilized the cells for FE-SEM analysis. The FE-SEM examination revealed the presence of nanoparticles on the surface of the recombinant *E. coli* (pBADCF) after exposure to 2 mM cobalt solution (Figure 3C). This result suggests that cobalt nanoparticles, with sizes ranging from 80 to 100 nm, primarily adhered to the cell wall. The EDS spectra exhibited peaks at 6.931 and 7.649 keV, corresponding to Co Kα1 and Co Kβ1, respectively, confirming the existence of cobalt nanoparticles within the strains. In contrast, the wild-type *E. coli* (DH5α) did not exhibit nanoparticle formation on the cell wall.

The recombinant *E. coli* strain displayed prominent cobalt salt nanoparticles on the membrane's surface. A study of cobalt adsorption indicated that the cell wall of the recombinant *E. coli* possessed multiple binding sites for cobalt ions on its surface. These ions on the cell wall can undergo reactions to form inorganic compounds that precipitate out of the solution. These precipitation sites can locally accumulate ions, enhance surface coverage, and facilitate ion clustering, forming solid nanoparticles on the cell wall. Previous research has demonstrated the ability of metal-binding peptides to biologically synthesize inorganic particles, including gold, platinum, silver, cobalt, and calcium carbonate.[35−39]

https://doi.org/10.1021/acsomega.3c10246
ACS Omega 2024, 9, 31373−31383

3.4. Synthesis of Cobalt Oxide Nanoparticles and Their Characterization. To synthesize cobalt oxide nanoparticles, cobalt-adsorbed *E. coli* (pBADCF) strains were subjected to calcination at different temperatures (400 °C, 500 °C, 600 °C, and 700 °C) to eliminate impurities and volatile substances. Higher temperatures were employed to convert the metal samples into oxides, followed by the recovery and subsequent analysis of the oxide nanoparticles using FE-SEM, Zeta potential, Zeta sizer, EDS, XRD, FT-IR, and Raman spectroscopy.

3.4.1. FE-SEM and EDS. SEM allowed the determination of the structures and shapes of the produced powders. The particles precipitated from cobalt exhibited a diverse range of sizes and forms, and their aggregation resulted in spherical formations. Notably, many of these particles exhibited an almost round shape. They measured between 60 and 150 nm in diameter, as depicted in Figure 4A. Some particle groups were substantial, featuring a dense packing of smaller particles, while others remained relatively small. Even in densely packed configurations, there were some observable gaps and minuscule voids within the product clusters.

This observation indicates that the product consisted of interconnected nanoparticles and microparticles, contributing to an irregular pattern. Moving from the sample's core to its surface, a noticeable void in the particle arrangement became evident, resulting in an uneven distribution of nanoparticles.

Figure 4A presents the EDS spectra for thermally treated nanoparticles at 500 °C. The spectra revealed that the synthesized Co_3O_4 sample primarily comprised cobalt (Co) and oxygen (O) components. Specifically, the initial peak corresponding to oxygen emerged at 0.5 keV, while cobalt was revealed at Co Kα1 (6.931 keV) and Co Kβ1 (7.649 keV).[40,41] The product contained cobalt and oxygen elements with a Co/O atomic ratio of approximately 3/3.97, consistent with the theoretical value for Co_3O_4. This observation underscores the remarkable purity of the Co_3O_4 nanoparticles.

3.4.2. Zeta Sizer and Zeta Potential. The mean size distribution and the Zeta potential of cobalt oxide nanoparticles were oxidized at a temperature of 500 °C and analyzed using a Zeta sizer Nano series analyzer. The average size of the cobalt oxide nanoparticle was 124.5 d.nm (Supplementary Figure S1). The cobalt oxide nanoparticles possess a little negative charge on their surface, as evidenced by the negative zeta potential of −8.4 (Supplementary Figure S2). This negative charge caused a repulsive interaction between the particles, crucial for the initial development of stability and interaction with biological molecules and cells. The average size of 124 d.nm suggests they fall within the typical range for effective nanoparticle delivery systems in cancer therapy. Particles with zeta potential values exceeding +25 mV or dropping below −25 mV are typically regarded as having a substantial degree of stability.[13] The presence of powerful electric charges hindered the aggregation process. The capping agent enhanced the stability of nanoparticles by inducing a negative charge on them.[13] The negative zeta potential of −8.4 is not a greater zeta potential, so there is a small quantity of aggregation between the nanoparticles, which is evident in SEM image Figure 4A. Greater charges result in increased stability, which avoids aggregation. The tiny particles were concealed by the larger ones, rendering them imperceptible utilizing the used method. The presence of larger particles caused light scattering, resulting in the obstruction of signals emitted by smaller particles.

3.4.3. XRD. Using XRD with a model X'Pert^3 and Co Kα radiation (λ = 1.54 Å) in the range (2θ) 10°−90°, the crystal structure was classified. Figure 4B shows that cobalt oxide film is polycrystalline. The Co_3O_4 samples (at 400 °C, 500 °C, 600 °C, 700 °C) exhibited typical diffraction peaks at 31.4, 36.8, 38.3, 44.9, 59.3, and 65.3, which correspond to the (220), (311), (222), (400), (511), and (440) planes, respectively, of the[42,43] crystalline structure of the three-dimensional spinel Co_3O_4 phase, signifying the creation of crystal-like Co_3O_4 (JCPDS Card no. 43−1003).[42]

3.4.4. FT-IR Spectroscopy. FT-IR was used to examine the calcinated particles at distinct temperatures to illustrate shifts in the functional groups of oxidized cobalt nanoparticles (Figure 4C). The band at 1623 cm^{-1} was associated with the angular distortion of adsorbed water molecules. C−O stretching vibrations caused a peak at 1023 cm^{-1}.[43] The peak at 2371 cm^{-1} was due to the irregular vibration (C = O) of CO_2 received from the air during the thermal annealing of metal oxides.[43] All the oxide samples' FT-IR spectra had the same distinctive peaks as pure cobalt oxide (PCO), indicating a comparable chemical bonding nature. The tiny bands at 566 and 665 cm^{-1} may have been OB3 (B−Co^{3+} in an octahedral site) and ABO (A−Co^{2+} in a tetrahedral site) vibrations, respectively, in the Co_3O_4 spinel matrix.[43]

3.4.5. Raman Spectroscopy. Raman spectroscopy was employed to investigate the characteristics of oxidized cobalt. This approach is sensitive to morphological and structural changes in oxidized cobalt nanoparticles, making it a helpful tool for determining catalyst composition (Figure 4D). The discovery of the Co_3O_4 spinel occurred due to three distinct peaks in the spectrum at 466 cm^{-1}, 508 cm^{-1}, and 672 cm^{-1}. The F_{2g} Raman vibration mode was attributed to the peaks at 508 cm^{-1}, while the E_g and A_{1g} vibration modes were allocated to the peaks at 466 and 672 cm^{-1}, respectively.[43] The small peaks, at 1350 cm^{-1}, were ascribed to the D band. The D band is assigned to the A_{1g} symmetry mode of k-point phonons.[44]

4. ANTICANCER EVALUATION OF Co_3O_4 NANOPARTICLES

After conducting extensive research spanning three decades, researchers have demonstrated that certain nanomedicines derived from nanoparticles possess the potential to effectively treat cancer, offering advantages such as high biocompatibility, precise targeting, and minimal toxicity.[45] Metal oxide nanoparticles, including many anticancer agents, have been investigated.[46] Recently, researchers have reported the anticancer activity of cobalt oxide nanoparticles, indicating their potential therapeutic value in cancer treatment.

One study revealed the targeting of gastric cancer (AGS) cells by the Co_3O_4 @ Glu/TSC nanoparticle complex, which could potentially serve as a drug delivery system, consistent with prior research findings.[47] Furthermore, cobalt oxide nanoparticles induced oxidative stress by generating reactive oxygen species (ROS). These nanoparticles also exhibit chemotherapeutic potential for combating invasive breast cancer cells.[7] Cobalt complexes are bound to DNA and facilitated spiral elongation. Cytotoxicity testing on the MCF-7 breast cancer cell line revealed that certain compounds displayed anticancer properties.[48] Furthermore, PMIDA-coated cobalt oxide nanoparticles significantly enhanced cellular adsorption, eradicating cancer cells in cytotoxicity experiments on T-cell lymphoma and oral carcinoma.[49] Biogenic cobalt oxide nanoparticles exhibited cytotoxic effects

https://doi.org/10.1021/acsomega.3c10246
ACS Omega 2024, 9, 31373−31383

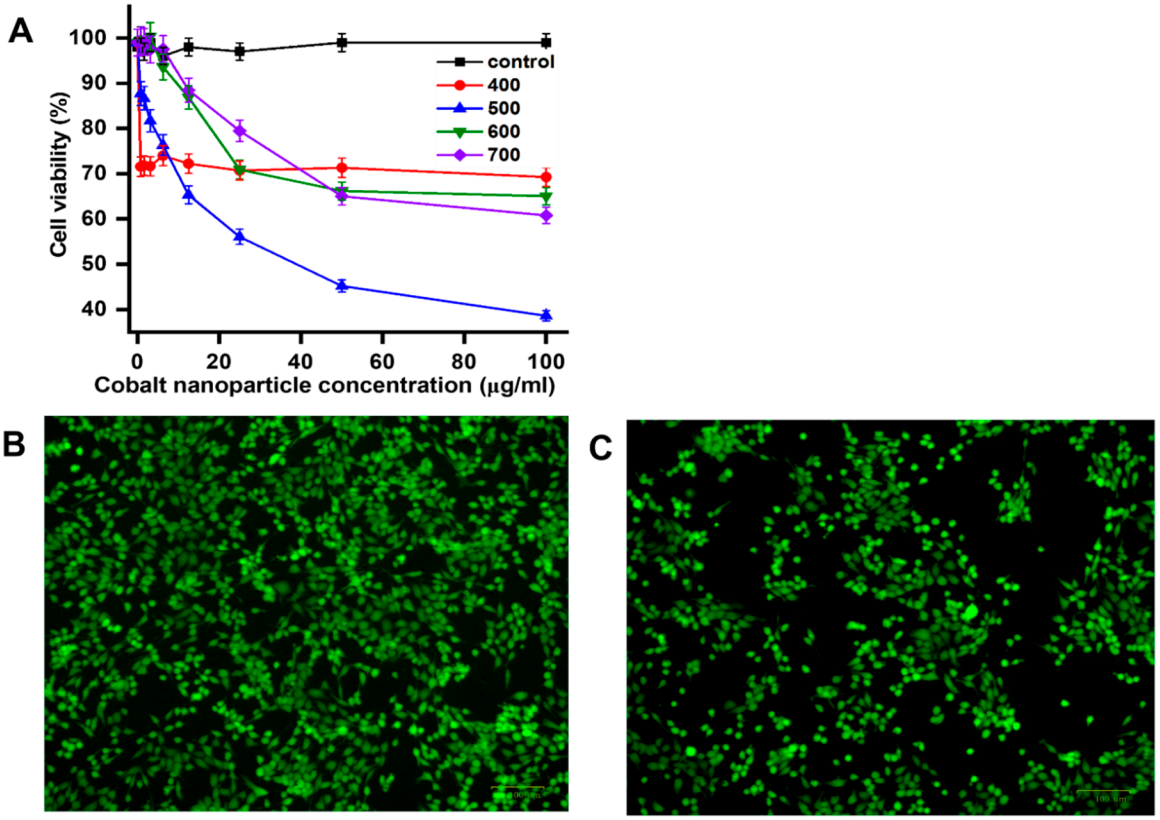

Figure 5. (A) Anticancer activity of cobalt oxide nanoparticle calcinated at different temperatures (400 °C, 500 °C, 600 °C, and 700 °C) from *E. coli* (pBADCF) adsorbed cobalt. Each line graph shows the mean value of five experiments. The error bars were calculated by dividing the standard deviation by the square root of the number of measurements. (B) Cell viability for the positive control. (C) Cell viability at 50 μg/mL of Co_3O_4 calcinated at 500 °C.

on HeLa cell lines, further affirming their potential as an anticancer agent.[50]

Our study employed the MTT assay to evaluate the cytotoxicity of cobalt oxide nanoparticles synthesized by calcinating the *E. coli* (pBADCF) strain with adsorbed cobalt at temperatures ranging from 400 to 700 °C. In this study, 1×10^4 4T1 tumor cells (triple-negative mouse breast cancer cell line) were initially incubated in a 96-well plate with 100 μL of growth medium and exposed to varying concentrations of cobalt oxide nanoparticles (0.78, 1.56, 3.13, 6.25, 12.5, 25, 50, and 100 μg/mL). The treated cells were then incubated at 37 °C with 5% CO_2 for 1 day, and the inhibitory concentration (IC_{50}) was determined based on the difference in viability between untreated and treated cells. The positive control exhibited a viability rate of approximately 98%. Cobalt oxide nanoparticles calcinated at 400 °C inhibited cell proliferation to about 70−75% (Figure 5A). Microscopic green fluorescent images of 4T1 cell lines are provided for the cell viability of the positive control (Figure 5B) and for cell viability inhibited at 50 μg/mL of cobalt oxide nanoparticles calcinated at 500 °C (Figure 5C). Even at a concentration of 100 μg, the cobalt oxide nanoparticles calcinated at 700 °C showed a viability of 60% and a significantly higher average proliferation rate of nearly 100% at lower concentrations. Cobalt oxide nanoparticles heated to 600 °C exhibited 100% viability at lower concentrations and only a 25% apoptosis rate at higher concentrations (100 g).

The nanoparticles synthesized at 500 °C demonstrated an IC_{50} value of 59 μg/mL, while samples synthesized at 400 °C, 600 °C, and 700 °C required 670 μg/mL, 116 μg/mL, and 110 μg/mL, respectively. Consequently, the sample synthesized at 500 °C exhibited more significant cytotoxicity than the others.

In comparison to cobalt oxide nanoparticles synthesized using the cochineal dye approach, the IC_{50} value of 2 mg/mL is significantly higher than the IC_{50} value of 59 μg/mL achieved with microbially synthesized 500 °C cobalt oxide nanoparticles using the same 4T1 cell lines.[49] The green synthesis of cobalt oxide nanoparticles using *Psidium guajava* leaf extract yielded even better IC_{50} values: 24.5 μg/mL for HCT116 cells and 29.5 μg/mL for MCF-7 cells.[51] Microbial synthesis of cobalt oxide nanoparticles using MRS-1 *Microbacterium* sp. resulted in 50% cell death at 100 mg/mL.[14] Another study showcased the anticancer potential of cobalt oxide nanoparticles against HT29 and SW620 cells, revealing IC_{50} values of 2.26 and 394.5 g/mL, respectively.[52] Compared to all other studies, our cobalt oxide nanoparticles, synthesized by genetically modified strains, exhibited higher apoptosis at lower concentrations. To fully uncover the medicinal potential of cobalt-Schiff-base complexes, comprehensive investigations of the structure−activity relationship are imperative. Although this molecule can induce DNA damage and cancer cell death, further research is needed to optimize its concentration.[53]

5. CONCLUSION

Recombinant bacteria have synthesized cobalt oxide nanoparticles with numerous applications, including use as catalysts for batteries in the medical sector and photocatalytic dye degradation. The continued utilization of whole-cell bio-

https://doi.org/10.1021/acsomega.3c10246
ACS Omega 2024, 9, 31373−31383

catalysis to create cobalt oxide nanoparticles with a cell surface display system remains valuable for environmental purposes. Molecular modeling and wet lab analysis were utilized to ensure an optimal design and enhance the activity of a specific peptide on the cell surface. This work synthesized and displayed cobalt-binding peptides on the cell surface using the OmpC anchoring motif in *E. coli* (pBADCF). These peptides exhibited a significantly higher cobalt recovery rate, averaging ≥2183 μmol/g DCW at pH 7 and a 2 mM Co concentration, than other peptides. Furthermore, FE-SEM was employed to examine the morphological characteristics of cobalt attached to recombinant cells. The zeta analyzer derived the size and zeta potential of the cobalt oxide nanoparticle oxidized at 500 °C. Numerous other reports have characterized and explored the potential applications of cobalt oxide nanoparticles obtained from peptides through calcination. Notably, when heated to 500 °C, the best oxide demonstrated a progressive mortality rate in cancer cells. However, further research is required to determine the appropriate concentration for biomedical applications.

■ ASSOCIATED CONTENT

Supporting Information

The Supporting Information is available free of charge at https://pubs.acs.org/doi/10.1021/acsomega.3c10246.

Supplementary Figure S1 showed the average size of the cobalt oxide nanoparticle oxidized at 500 °C. The cobalt oxide nanoparticle was analyzed with a Zeta sizer analyzer. Supplementary Figure S2 showed the average Zeta potential of the cobalt oxide nanoparticle oxidized at 500 °C. The cobalt oxide nanoparticle was analyzed with a Zeta sizer analyzer (PDF)

■ AUTHOR INFORMATION

Corresponding Author

Soon Ho Hong − *Department of Chemical Engineering, University of Ulsan, Ulsan 44610, Republic of Korea;* orcid.org/0000-0003-0035-7117; Email: shhong@ulsan.ac.kr

Authors

Ashokkumar Kumaravel − *Department of Chemical Engineering, University of Ulsan, Ulsan 44610, Republic of Korea*

Turbasu Sengupta − *Department of Chemical Engineering, University of Ulsan, Ulsan 44610, Republic of Korea;* orcid.org/0000-0003-3562-4414

Padmanaban Sathiyamoorthy − *Department of Medical Nanotechnology, School of Chemical & Biotechnology, SASTRA Deemed University, Tamil Nadu 613401, India*

Jaehoon Jeong − *Department of Chemical Engineering, University of Ulsan, Ulsan 44610, Republic of Korea*

Sung Gu Kang − *Department of Chemical Engineering, University of Ulsan, Ulsan 44610, Republic of Korea;* orcid.org/0000-0003-1112-7077

Complete contact information is available at: https://pubs.acs.org/10.1021/acsomega.3c10246

Author Contributions

Ashokkumar Kumaravel: Methodology, Formal analysis, Validation, Investigation, Writing−review and editing. **Turbasu Sengupta:** Methodology, Bioinformatic analysis, Investigation. **Jeong Jae Hoon:** Methodology, Formal analysis, Investigation. **Padmanaban Sathiyamoorthy:** Methodology, Formal analysis, Investigation. **Sung Gu Kang:** Methodology, Bioinformatic analysis, Investigation. **Soon Ho Hong:** Conceptualization, Supervision, Visualization, Methodology, Formal analysis, Validation, Investigation, Writing−review and editing.

Notes

The authors declare no competing financial interest.

■ ACKNOWLEDGMENTS

This work was supported by a Korea Institute for Advancement of Technology (KIAT) grant funded by the Korea government (MOTIE) (P0023727) and Regional Innovation Strategy (RIS) through the National Research Foundation of Korea (NRF) funded by the Ministry of Education (MOE) (2021RIS-003).

■ REFERENCES

(1) Pourret, O.; Faucon, M.-P. Cobalt. In *Encyclopedia of Earth Sciences Series*; 2018; pp 291−294.

(2) Prathna, T. C.; Mathew, L.; Chandrasekaran, N.; Raichur, A. M.; Mukherjee, A. Biomimetic Synthesis of Nanoparticles: Science, Technology & Applicability. In *Biomimetics*; Mukherjee, A., Ed.; IntechOpen: Rijeka, 2010; p Ch. 1.

(3) Bibi, I.; Nazar, N.; Iqbal, M.; Kamal, S.; Nawaz, H.; Nouren, S.; Safa, Y.; Jilani, K.; Sultan, M.; Ata, S.; Rehman, F.; Abbas, M. Green and Eco-Friendly Synthesis of Cobalt-Oxide Nanoparticle: Characterization and Photo-Catalytic Activity. *Advanced Powder Technology* **2017**, *28* (9), 2035−2043.

(4) Jang, E.; Ryu, B. H.; Shim, H.-W.; Ju, H.; Kim, D.-W.; Kim, T. D. Adsorption of Microbial Esterases on Bacillus Subtilis-Templated Cobalt Oxide Nanoparticles. *Int. J. Biol. Macromol.* **2014**, *65*, 188−192.

(5) AbdelRahim, K.; Mahmoud, S. Y.; Ali, A. M.; Almaary, K. S.; Mustafa, A. E.-Z. M. A.; Husseiny, S. M. Extracellular Biosynthesis of Silver Nanoparticles Using Rhizopus Stolonifer. *Saudi J. Biol. Sci.* **2017**, *24* (1), 208−216.

(6) Dong, H.; Meininger, A.; Jiang, H.; Moon, K.-S.; Wong, C. P. Magnetic Nanocomposite for Potential Ultrahigh Frequency Microelectronic Application. *J. Electron. Mater.* **2007**, *36* (5), 593−597.

(7) Jarestan, M.; Khalatbari, K.; pouraei, A.; Sadat Shandiz, S. A.; Beigi, S.; Hedayati, M.; Majlesi, A.; Akbari, F.; Salehzadeh, A. Preparation, Characterization, and Anticancer Efficacy of Novel Cobalt Oxide Nanoparticles Conjugated with Thiosemicarbazide. *3 Biotech* **2020**, *10* (5), 230.

(8) Puche, M.; Liu, L.; Concepción, P.; Sorribes, I.; Corma, A. Tuning the Catalytic Performance of Cobalt Nanoparticles by Tungsten Doping for Efficient and Selective Hydrogenation of Quinolines under Mild Conditions. *ACS Catal.* **2021**, *11* (13), 8197−8210.

(9) Parkes, L. M.; Hodgson, R.; Lu, L. T.; Tung, L. D.; Robinson, I.; Fernig, D. G.; Thanh, N. T. K. Cobalt Nanoparticles as a Novel Magnetic Resonance Contrast Agent—Relaxivities at 1.5 and 3 T. *Contrast Media Mol. Imaging* **2008**, *3* (4), 150−156.

(10) Farkaš, B.; Terranova, U.; de Leeuw, N. H. The Mechanism Underlying the Functionalisation of Cobalt Nanoparticles by Carboxylic Acids: A First-Principles Computational Study. *J. Mater. Chem. B* **2021**, *9* (24), 4915−4928.

(11) De, D.; Upadhyay, P.; Das, A.; Ghosh, A.; Adhikary, A.; Goswami, M. M. Studies on Cancer Cell Death through Delivery of Dopamine as Anti-Cancer Drug by a Newly Functionalized Cobalt Ferrite Nano-Carrier. *Colloids Surf. A Physicochem Eng. Asp* **2021**, *627*, 127202.

(12) Jincy, C. S.; Meena, P. Synthesis, Characterization, and NH3 Gas Sensing Application of Zn Doped Cobalt Oxide Nanoparticles. *Inorg. Chem. Commun.* **2020**, *120*, 108145.

(13) Vijayanandan, A. S.; Balakrishnan, R. M. Biosynthesis of Cobalt Oxide Nanoparticles Using Endophytic Fungus Aspergillus Nidulans. *J. Environ. Manage* **2018**, *218*, 442−450.
(14) Sundararaju, S.; Arumugam, M.; Bhuyar, P. Microbacterium Sp. MRS-1, a Potential Bacterium for Cobalt Reduction and Synthesis of Less/Non-Toxic Cobalt Oxide Nanoparticles (Co_3O_4). *Beni Suef Univ J. Basic Appl. Sci.* **2020**, *9* (1), 44.
(15) Mubraiz, N.; Bano, A.; Mahmood, T.; Khan, N. Microbial and Plant Assisted Synthesis of Cobalt Oxide Nanoparticles and Their Antimicrobial Activities. *Agronomy 2021, Vol. 11, Page 1607* **2021**, *11* (8), 1607.
(16) Jang, E.; Shim, H.-W.; Ryu, B. H.; An, D. R.; Yoo, W. K.; Kim, K. K.; Kim, D.-W.; Kim, T. D. Preparation of Cobalt Nanoparticles from Polymorphic Bacterial Templates: A Novel Platform for Biocatalysis. *Int. J. Biol. Macromol.* **2015**, *81*, 747−753.
(17) Iravani, S.; Varma, R. S. Sustainable Synthesis of Cobalt and Cobalt Oxide Nanoparticles and Their Catalytic and Biomedical Applications. *Green Chem.* **2020**, *22* (9), 2643−2661.
(18) Marimuthu, S.; Rahuman, A. A.; Kirthi, A. V.; Santhoshkumar, T.; Jayaseelan, C.; Rajakumar, G. Eco-Friendly Microbial Route to Synthesize Cobalt Nanoparticles Using Bacillus Thuringiensis against Malaria and Dengue Vectors. *Parasitol Res.* **2013**, *112* (12), 4105−4112.
(19) Lee, S. Y.; Choi, J. H.; Xu, Z. Microbial Cell-Surface Display. *Trends Biotechnol* **2003**, *21* (1), 45−52.
(20) Ravikumar, S.; Yoo, I.; Lee, S. Y.; Hong, S. H. Construction of Copper Removing Bacteria Through the Integration of Two-Component System and Cell Surface Display. *Appl. Biochem. Biotechnol.* **2011**, *165* (7), 1674−1681.
(21) Bae, W.; Wu, C. H.; Kostal, J.; Mulchandani, A.; Chen, W. Enhanced Mercury Biosorption by Bacterial Cells with Surface-Displayed MerR. *Appl. Environ. Microbiol.* **2003**, *69* (6), 3176−3180.
(22) Bae, W.; Mulchandani, A.; Chen, W. Cell Surface Display of Synthetic Phytochelatins Using Ice Nucleation Protein for Enhanced Heavy Metal Bioaccumulation. *J. Inorg. Biochem* **2002**, *88* (2), 223−227.
(23) Lamiable, A.; Thevenet, P.; Rey, J.; Vavrusa, M.; Derreumaux, P.; Tuffery, P. PEP-FOLD3: Faster de Novo Structure Prediction for Linear Peptides in Solution and in Complex. *Nucleic Acids Res.* **2016**, *44* (W1), W449−W454.
(24) Shen, Y.; Maupetit, J.; Derreumaux, P.; Tufféry, P. Improved PEP-FOLD Approach for Peptide and Miniprotein Structure Prediction. *J. Chem. Theory Comput* **2014**, *10* (10), 4745−4758.
(25) Thévenet, P.; Shen, Y.; Maupetit, J.; Guyon, F.; Derreumaux, P.; Tufféry, P. PEP-FOLD: An Updated de Novo Structure Prediction Server for Both Linear and Disulfide Bonded Cyclic Peptides. *Nucleic Acids Res.* **2012**, *40* (W1), W288−W293.
(26) Zhang, J.; Dolg, M. ABCluster: The Artificial Bee Colony Algorithm for Cluster Global Optimization. *Phys. Chem. Chem. Phys.* **2015**, *17* (37), 24173−24181.
(27) Zhang, J.; Dolg, M. Global Optimization of Clusters of Rigid Molecules Using the Artificial Bee Colony Algorithm. *Phys. Chem. Chem. Phys.* **2016**, *18* (4), 3003−3010.
(28) Zhang, J.; Glezakou, V.-A. Global Optimization of Chemical Cluster Structures: Methods, Applications, and Challenges. *Int. J. Quantum Chem.* **2021**, *121* (7), No. e26553.
(29) Frisch, M. J., et al. *Gaussian 16*, Rev. C.01; Gaussian: Wallingford, CT, 2016.
(30) Stewart, J. J. P. Optimization of Parameters for Semiempirical Methods V: Modification of NDDO Approximations and Application to 70 Elements. *J. Mol. Model* **2007**, *13* (12), 1173−1213.
(31) Marenich, A. V.; Cramer, C. J.; Truhlar, D. G. Universal Solvation Model Based on Solute Electron Density and on a Continuum Model of the Solvent Defined by the Bulk Dielectric Constant and Atomic Surface Tensions. *J. Phys. Chem. B* **2009**, *113* (18), 6378−6396.
(32) Sun, X.; Xiao, C.; Ge, R.; Yin, X.; Li, H.; Li, N.; Yang, X.; Zhu, Y.; He, X.; He, Q.-Y. Putative Copper- and Zinc-Binding Motifs in Streptococcus Pneumoniae Identified by Immobilized Metal Affinity Chromatography and Mass Spectrometry. *Proteomics* **2011**, *11* (16), 3288−3298.
(33) Li, C.-C.; Chung, H.-P.; Wen, H.-W.; Chang, C.-T.; Wang, Y.-T.; Chou, F.-I. The Radiation Resistance and Cobalt Biosorption Activity of Yeast Strains Isolated from the Lanyu Low-Level Radioactive Waste Repository in Taiwan. *J. Environ. Radioact* **2015**, *146*, 80−87.
(34) Jung, H.; Inaba, Y.; Jiang, V.; West, A. C.; Banta, S. Engineering Polyhistidine Tags on Surface Proteins of Acidithiobacillus Ferrooxidans: Impact of Localization on the Binding and Recovery of Divalent Metal Cations. *ACS Appl. Mater. Interfaces* **2022**, *14* (8), 10125−10133.
(35) Lee, H.; Lee, E. M.; Reginald, S. S.; Chang, I. S. Peptide Sequence-Driven Direct Electron Transfer Properties and Binding Behaviors of Gold-Binding Peptide-Fused Glucose Dehydrogenase on Electrode. *iScience* **2021**, *24* (11), 103373.
(36) Pramounmat, N.; Yan, K.; Wolf, J.; Renner, J. N. Platinum-Binding Peptides: Understanding of Selective Binding and Multifunctionality. *Multifunctional Materials* **2022**, *5* (1), 012002.
(37) Hughes, Z. E.; Nguyen, M. A.; Wang, J.; Liu, Y.; Swihart, M. T.; Poloczek, M.; Frazier, P. I.; Knecht, M. R.; Walsh, T. R. Tuning Materials-Binding Peptide Sequences toward Gold- and Silver-Binding Selectivity with Bayesian Optimization. *ACS Nano* **2021**, *15* (11), 18260−18269.
(38) Cho, Y.; Mirzapour-Kouhdasht, A.; Yun, H.; Park, J. H.; Min, H. J.; Lee, C. W. Development of Cobalt-Binding Peptide Chelate from Human Serum Albumin: Cobalt-Binding Properties and Stability. *Int. J. Mol. Sci.* **2022**, *23* (2), 719.
(39) Finney, A. R.; Innocenti Malini, R.; Freeman, C. L.; Harding, J. H. Amino Acid and Oligopeptide Effects on Calcium Carbonate Solutions. *Cryst. Growth Des* **2020**, *20* (5), 3077−3092.
(40) Pal Singh, R. P.; Hudiara, I. S.; Bhushan Rana, S. Effect of Calcination Temperature on the Structural, Optical and Magnetic Properties of Pure and Fe-Doped ZnO Nanoparticles. *Materials Science-Poland* **2016**, *34* (2), 451−459.
(41) Yin, X.; Tang, C.; Zhang, L.; Yu, Z. G.; Gong, H. Chemical Insights into the Roles of Nanowire Cores on the Growth and Supercapacitor Performances of Ni-Co-O/Ni(OH)2 Core/Shell Electrodes. *Sci. Rep* **2016**, *6* (1), 21566.
(42) Liu, F.; Su, H.; Jin, L.; Zhang, H.; Chu, X.; Yang, W. Facile Synthesis of Ultrafine Cobalt Oxide Nanoparticles for High-Performance Supercapacitors. *J. Colloid Interface Sci.* **2017**, *505*, 796−804.
(43) Naveen, A. N.; Selladurai, S. Investigation on Physiochemical Properties of Mn Substituted Spinel Cobalt Oxide for Supercapacitor Applications. *Electrochim. Acta* **2014**, *125*, 404−414.
(44) Wang, X.; Song, L.; Yang, H.; Xing, W.; Lu, H.; Hu, Y. Cobalt Oxide/Graphene Composite for Highly Efficient CO Oxidation and Its Application in Reducing the Fire Hazards of Aliphatic Polyesters. *J. Mater. Chem.* **2012**, *22* (8), 3426−3431.
(45) Li, W.; Cao, Z.; Yu, L.; Huang, Q.; Zhu, D.; Lu, C.; Lu, A.; Liu, Y. Hierarchical Drug Release Designed Au @PDA-PEG-MTX NPs for Targeted Delivery to Breast Cancer with Combined Photothermal-Chemotherapy. *J. Nanobiotechnology* **2021**, *19* (1), 143.
(46) Vinardell, M. P.; Mitjans, M. Antitumor Activities of Metal Oxide Nanoparticles. *Nanomaterials (Basel)* **2015**, *5* (2), 1004−1021.
(47) Thamilarasan, V.; Sengottuvelan, N.; Sudha, A.; Srinivasan, P.; Chakkaravarthi, G. Cobalt(III) Complexes as Potential Anticancer Agents: Physicochemical, Structural, Cytotoxic Activity and DNA/Protein Interactions. *J. Photochem. Photobiol. B* **2016**, *162*, 558−569.
(48) Chattopadhyay, S.; Chakraborty, S. P.; Laha, D.; Baral, R.; Pramanik, P.; Roy, S. Surface-Modified Cobalt Oxide Nanoparticles: New Opportunities for Anti-Cancer Drug Development. *Cancer Nanotechnol* **2012**, *3* (1−6), 13−23.
(49) Goudarzi, M.; Salavati-Niasari, M. Synthesis, Characterization and Evaluation of Co_3O_4 Nanoparticles Toxicological Effect; Synthesized by Cochineal Dye via Environment Friendly Approach. *J. Alloys Compd.* **2019**, *784*, 676−685.

https://doi.org/10.1021/acsomega.3c10246
ACS Omega 2024, 9, 31373−31383

(50) Koyyati, R.; Rao Kudle, K.; Rudra Manthur Padigya, P. Evaluation of Antibacterial and Cytotoxic Activity of Green Synthesized Cobalt Nanoparticles Using Raphanus Sativus Var. *Longipinnatus Leaf Extract* **2016**, *9*, 466−472.
(51) Govindasamy, R.; Raja, V.; Singh, S.; Govindarasu, M.; Sabura, S.; Rekha, K.; Rajeswari, V. D.; Alharthi, S. S.; Vaiyapuri, M.; Sudarmani, R.; Jesurani, S.; Venkidasamy, B.; Thiruvengadam, M. Green Synthesis and Characterization of Cobalt Oxide Nanoparticles Using Psidium Guajava Leaves Extracts and Their Photocatalytic and Biological Activities. *Molecules 2022, Vol. 27, Page 5646* **2022**, *27* (17), 5646.
(52) Khan, S.; Ansari, A. A.; Khan, A. A.; Ahmad, R.; Al-Obaid, O.; Al-Kattan, W. In Vitro Evaluation of Anticancer and Antibacterial Activities of Cobalt Oxide Nanoparticles. *JBIC Journal of Biological Inorganic Chemistry* **2015**, *20* (8), 1319−1326.
(53) Munteanu, C. R.; Suntharalingam, K. Advances in Cobalt Complexes as Anticancer Agents. *Dalton Transactions* **2015**, *44* (31), 13796−13808.

https://doi.org/10.1021/acsomega.3c10246
ACS Omega 2024, 9, 31373−31383